


RAPID COMMUNICATION

Hydrogen response to high-density dislocations in bulk perovskite oxide SrTiO₃

Xufei Fang¹  | Lars Dörrer² | Svetlana Korneychuk^{1,3,4} | Maria Vrellou¹ | Alexander Welle^{4,5} | Stefan Wagner¹ | Astrid Pundt¹ | Harald Schmidt² | Christoph Kirchlechner¹

¹Institute for Applied Materials, Karlsruhe Institute of Technology, Karlsruhe, Germany

²Institute of Metallurgy, Solid-State-Kinetics Group, Clausthal University of Technology, Clausthal-Zellerfeld, Germany

³Institute of Nanotechnology, Karlsruhe Institute of Technology, Eggenstein-Leopoldshafen, Germany

⁴KNMFi, Karlsruhe Institute of Technology, Karlsruhe, Germany

⁵Institute of Functional Interfaces, Karlsruhe Institute of Technology, Eggenstein-Leopoldshafen, Germany

Correspondence

Xufei Fang, Institute for Applied Materials, Karlsruhe Institute of Technology, 76131 Karlsruhe, Germany.
Email: xufei.fang@kit.edu

Harald Schmidt, Institute of Metallurgy, Solid-State-Kinetics Group, Clausthal University of Technology, 38678 Clausthal-Zellerfeld, Germany.
Email: harald.schmidt@tu-clausthal.de

Funding information

European Research Council, Grant/Award Numbers: 101043969, 101076167; Karlsruhe Institute of Technology; KIT-YIN Grant

Abstract

Hydrogen plays an increasingly important role in green energy technologies. For instance, proton-conducting oxides with high performance for fuel cell components or electrolyzers need to be developed. However, this requires a fundamental understanding of hydrogen-defects interactions. Although point defects and grain boundaries in oxides have been extensively studied, the role of dislocations as line defects remains less understood, primarily due to the challenge for effective dislocation engineering in brittle oxides. In this work, we demonstrate the impact of dislocations in bulk single-crystal perovskite oxide SrTiO₃ on hydrogen uptake and diffusion using deuterium as tracer. Dislocations with a high density up to $\sim 10^{14}/\text{m}^2$ were mechanically introduced at room temperature. Exposing this dislocation-rich region and the reference regions (with a dislocation density of $\sim 10^{10}/\text{m}^2$) to deuterium at 400°C for 1 h, followed by secondary ion mass spectrometry measurements, we observed a ~ 100 times increase in deuterium incorporation in the dislocation-rich region. The result suggests that dislocations in oxides can act as an effective reservoir for deuterium. This proof-of-concept brings new insights into the emerging hydrogen-dislocation interactions in functional oxides.

KEYWORDS

diffusion, dislocation, hydrogen, oxide, secondary ion mass spectrometry

This is an open access article under the terms of the [Creative Commons Attribution](https://creativecommons.org/licenses/by/4.0/) License, which permits use, distribution and reproduction in any medium, provided the original work is properly cited.

© 2025 The Author(s). *Journal of the American Ceramic Society* published by Wiley Periodicals LLC on behalf of American Ceramic Society.

1 | INTRODUCTION

Hydrogen plays an increasingly important role due to its high societal impact in green energy technologies, such as hydrogen production and storage for energy conversion, green steels manufacturing for CO₂ reduction,¹ and energy-efficient computing.² Parallel to the extensive efforts in understanding hydrogen embrittlement in metallic materials for hydrogen storage and transportation, developing proton-conducting oxides with high performance for electrolyzers (for hydrogen production) and fuel cells (for hydrogen consumption) is sharing a fair fraction of scientific and economic weight. This requires fundamental understanding of hydrogen-defects interactions in oxides. So far, the majority of defect engineering efforts have been focused on point defects (e.g., oxygen vacancy tuning³) or grain boundaries as 2D defects (e.g., promoting the acceptor dopants segregation⁴). Another major defect type, dislocations as line defects in proton-conducting oxides or for hydrogen production, has rarely been considered, primarily due to the perception that ceramics are brittle and do not exhibit dislocation activities. This conventional picture is being revisited in recent years, as an increasing number of ceramics are being demonstrated for dislocation-mediated plastic deformation at room temperature up to meso/macroscale,⁵ as well as the dislocation-tuned functional and mechanical properties.^{6–9}

Dislocations as line defects can not only carry plastic deformation but also may act as fast diffusion paths for hydrogen.¹⁰ In the meantime, novel proofs-of-concepts have been put forward showcasing the enhanced hydrogen production rate (via water splitting) in functional oxides such as TiO₂ nanoparticles¹¹ and bulk BaTiO₃¹² with preengineered dislocations. Enhancement in proton conductivity due to misfit dislocations has also been reported via strain engineering in thin oxide films.^{13,14} Nevertheless, these studies require delicate processing procedures at the expense of high energy cost, for example, high-temperature bulk compression at 1150°C with an intermediate dislocation density of $\sim 10^{12}/\text{m}^2$,¹² or have a limited degree of controlling the dislocations in nanoparticles or at the interfaces of thin films. In terms of hydrogen-dislocation interaction (for instance, segregation, trapping, and diffusion) in functional oxides, the basic understanding remains far less developed.^{10,15,16} To this end, the first challenge is how to effectively and efficiently engineer high-density dislocations, preferably with much higher density than previously achieved,¹² in a large volume of material.

In this study, we aim to address the following questions: How does hydrogen respond to high-density dislocations in a bulk oxide, provided that the dislocations can be successfully engineered? Are these dislocations stable at

elevated temperatures for potential operation scenarios in, for example, solid oxide cells? In what follows, we adopted single-crystal SrTiO₃ as a prototypical perovskite oxide, which exhibits room-temperature dislocation plasticity in bulk compression¹⁷ and allows for efficient dislocation imprinting with high densities up to $\sim 10^{14}/\text{m}^2$ at room temperature.^{8,18} Then the sample, containing dislocation-rich as well as reference undeformed regions, was exposed to a hydrogen isotope, deuterium-rich environment at elevated temperatures, followed by secondary ion mass spectrometry (SIMS) measurements to assess the deuterium content and diffusion profile.

2 | RESULTS AND ANALYSES

2.1 | Dislocation engineering and visualization

A nominally undoped SrTiO₃ single crystal with (0 0 1) surface orientation was used (Alineason GmbH, Frankfurt am Main, Germany). Starting with a sample dimension of 5 mm × 5 mm × 1 mm, we mechanically imprinted dislocations in an area of about 2.5 × 2.5 mm² (Figure 1A), which is suitable for SIMS measurement. The dislocations were introduced by cyclic scratching the sample surface at room temperature¹⁹ with a Brinell indenter of a diameter of 2.5 mm and a normal load of 1 kg. The depth of the dislocations induced using this method extends beyond 50 μm.²⁰ Each individual wear track (Figure 1A,B) has a maximum depth of ~ 300 nm over ~ 130 μm¹⁹, yielding a nominally flat surface after scratching. Contrasting the reference region that has a dislocation density of $\sim 10^{10}/\text{m}^2$,²¹ high-density dislocations ($\sim 10^{14}/\text{m}^2$) were successfully generated in the scratch track after 10 passes of scratching, as evidenced by the TEM (transmission electron microscopy) observation of the cross section (Figure 1C) along the scratch track (Figure 1B). The dislocations are primarily aligned 45° with respect to the surface, corresponding to the activated {1 1 0} <1 1 0> slip systems in (0 0 1) SrTiO₃ at room temperature.^{18,22} Within the TEM field of view (deeper than 3 μm), the dislocations are distributed homogeneously along the depth in the near-surface region. No amorphization was detected in the heavily deformed region, which remains in single-crystal form as confirmed by the TEM diffraction pattern.

2.2 | Deuterium incorporation and SIMS measurements

We used deuterium (D) as a tracer for a better distinction from the hydrogen (H) background. D uptake was achieved

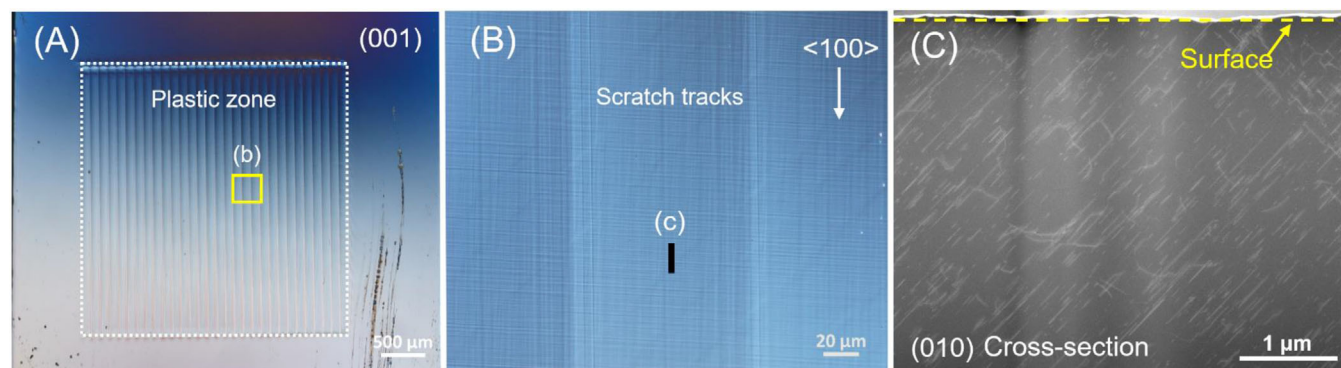


FIGURE 1 Visualization of the plastic zone and dislocations: (A) overview of the large plastic zone generated by overlapping the scratch tracks on the (0 0 1) surface. (B) Zoomed-in view of three scratch tracks in parallel, corresponding to the yellow rectangle in (A). (C) Annular dark field (ADF) STEM image of the cross-sectional region, lifted out at the surface, as indicated by the black line in (B).

by annealing the samples in a furnace at 400°C for 1 h in a wet O₂/D₂O atmosphere (bubbler at room temperature). The furnace works under oxidizing conditions using an oxygen flow of 6 L/h saturated with D₂O. D₂O dissociates and D is incorporated into the material that presumably leads to the formation of hydroxyl (–OD) groups²³. Oxygen vacancies may be involved in the incorporation process,²⁴ and discussions will follow. The temperature of 400°C was adopted to accelerate the D uptake without altering the dislocation structure, which will be confirmed later in the experiments. Hydrogen isotope (H and D) selective SIMS measurements (Cameca IMS-3F/4F) in depth profile mode were performed on the sample surface before and after the sample exposure to D₂O. An O[–] primary ion beam (14.5 keV, 30–90 nA) was used. The sputtered area was about 250 μm × 250 μm, wherefrom 20% in the center was gated for further signal processing in a double-focused mass spectrometer. In depth profiling mode, the secondary ion intensities of H⁺ and D⁺ ions were recorded as a function of sputtering time. Depth calibration was obtained by measuring the crater depth with a mechanical surface profiler (Tencor, Alphastep). To ensure a direct comparison, the tests were performed on the same sample containing both the dislocation-rich and dislocation-scarce regions (see Figure 1A). Note that the isotopes H (¹H) and D (²H) are chemically identical (neglecting the isotope effect), and the intensity of the respective SIMS signals (I_H and I_D) is converted to calculate the relative D fraction to $X_D = I_D / (I_H + I_D)$.

As illustrated in Figure 2A, prior to D₂O exposure, the relative deuterium fraction of the regions with a high dislocation density of $\sim 10^{14}/\text{m}^2$ (dislocation-rich) and a low dislocation density of $\sim 10^{10}/\text{m}^2$ (reference) is identical, overlapping with the natural isotope background of $X_D \sim 1.5 \times 10^{-4}$.²⁵ This serves as a benchmarking test. After D₂O exposure (Figure 2B), the relative deuterium fraction is enhanced by a factor of ~ 100 in the

dislocation-rich region to a depth of up to 70 nm, whereas in the region without dislocations, it stays close to the natural background. This indicates that an additional amount of deuterium is incorporated into the sample in the dislocation-rich region. The increase of the relative deuterium fraction at the sample surface for depths below ~ 10 nm indicates a modified surface structure (which is known for ABO₃-type perovskite oxides²⁶ even without treatment in a hydrogen-rich environment), where the deuterium may be more easily incorporated for both cases. This could be caused by the formation of a thin space charge layer at the surface²⁷ or near-surface reconstruction after annealing in the presence of deuterium, where a higher oxygen vacancy concentration is formed.²⁸ The conditions of SIMS measurements are the same for dislocation-free and dislocation-rich regions. However, as can be seen from Figure 2, the probed depths for the reference and dislocation-rich regions are consistently different, before and after D exposure. The difference can be explained by a higher sputter yield (material removal rate) due to the severely distorted lattices in dislocation-rich regions compared to the reference regions.

2.3 | Diffusivity of deuterium in the dislocation-rich region

To gain insight into the modification of the deuterium fraction at larger depths and to determine the diffusivity of deuterium in the dislocation-rich region, long-time SIMS measurement was performed to depths of ~ 2700 nm using a higher primary beam intensity. This depth is within the TEM field of view, which visualized a uniform dislocation density along the depth within ~ 3000 nm (Figure 1C). As illustrated in Figure 3A, we observe a continuous penetration of deuterium into the sample in the dislocation-rich region and a decrease of the deuterium fraction over two

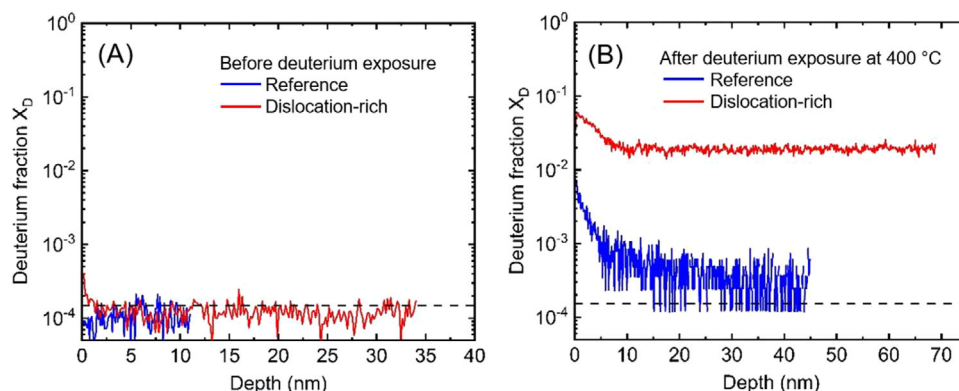


FIGURE 2 Deuterium fraction measured on a nominally undoped SrTiO₃ single crystal by secondary ion mass spectrometry (SIMS) in areas with a high dislocation density of $\sim 10^{14}/\text{m}^2$ (dislocation-rich) and a low dislocation density $\sim 10^{10}/\text{m}^2$ (reference): (A) before exposure to D₂O. (B) After exposure to D₂O at 400 °C for 1 h. The natural isotope background of $\sim 1.5 \times 10^{-4}$ is indicated by the black dashed line.

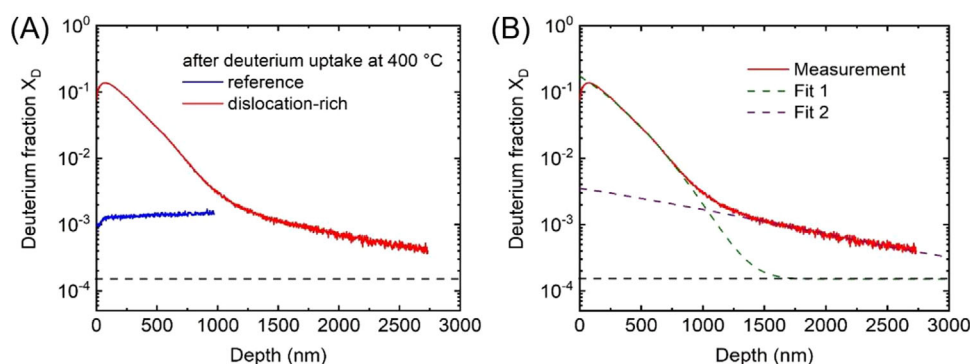


FIGURE 3 (A) Deuterium fraction, X_D , as a function of depth for larger depths for the dislocation-rich and the reference region without dislocations. (B) Experimental data of (A) for the dislocation-rich region, with fitting curves according to Equation (1). Shown are two fits for the depth between 70 and 900 nm (Fit 1) and the tail for depth between 1500 and 2700 nm (Fit 2). The natural isotope background is indicated by the black dashed line in both (A) and (B).

orders of magnitude. In contrast, the reference region reveals a constant low level of D fraction up to 1000 nm.

In the range between 70 and 900 nm (the near-surface data were cut off to avoid compositional uncertainties caused by surface roughness induced by the scratching), the diffusion profile can be described²⁹ by the following solution of Fick's second law using the boundary condition at the surface $-D \frac{\partial C}{\partial x} = K (c_0 - c_s)$, $x = 0$ ³⁰:

$$c(x, t) - c_\infty = (c_0 - c_\infty) \left[\operatorname{erfc} \left(\frac{x}{\sigma} \right) - \exp \left(2 \frac{x}{\sigma} \sqrt{\frac{t}{\tau}} + \frac{t}{\tau} \right) \operatorname{erfc} \left(\frac{x}{\sigma} + \sqrt{\frac{t}{\tau}} \right) \right] \quad (1)$$

with c_s being the actual surface concentration, $\sigma = 2\sqrt{D_D t}$, and $\tau = D_D/K^2$, whereas $c_0 = 0.95$ is the relative fraction of D in the source, $c_\infty = 1.5 \times 10^{-4}$ is the natural abundance of D in the single crystal, D_D is the deuterium

diffusivity, and K is the surface-exchange coefficient. The quantity K describes the kinetics of the exchange between the heavy water source and the crystal. We obtain from least-squares fitting values of $D_D = 2.7 \times 10^{-17} \text{ m}^2/\text{s}$ and $K = 1.7 \times 10^{-11} \text{ m/s}$. The relative error of the diffusivity is about 30% resulting from the determination of the crater depth. The deuterium diffusivity is rather low compared to other perovskite oxides like undeformed LiNbO₃, where such diffusivities were already reached at about 250 °C.³¹ This is surprising because the present diffusion of hydrogen in SrTiO₃ along dislocations is expected to be fast. We speculate that trapping effects of other types of defects may play a considerable role, as will be discussed later.

The fitting curve (Fit 1) in Figure 3B does not capture the long tail of the SIMS signal at depths higher than 900 nm, which hints to a second faster diffusion process responsible for transporting deuterium in low amounts deeper into the sample. Fitting of this region between 1500 and 2700 nm with Equation (1) results in a higher diffusivity of $D_D = 4.5 \times 10^{-16} \text{ m}^2/\text{s}$ ($K = 1.1 \times 10^{-12} \text{ m/s}$). This

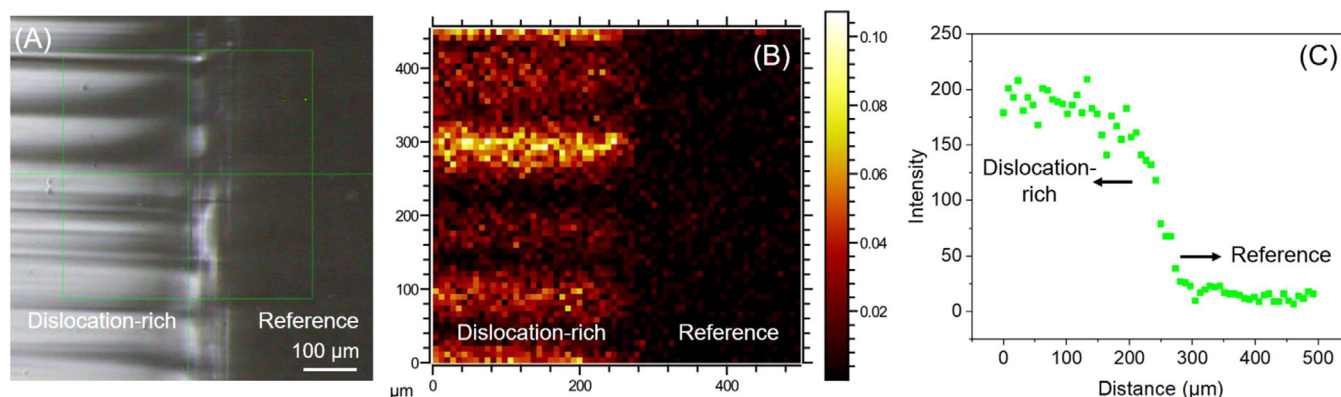


FIGURE 4 Direct correlation between the (A) optical image, (B) D fraction map, and (C) the quantified relative D intensity across the dislocation-rich and reference area. Note (B) corresponds to the large green rectangle indicated in (A).

result possibly indicates that diffusion along different types of dislocation structure may exist. Future investigations will include time- and temperature-dependent exposure to D_2O as well as systematic analysis of the dislocation mesostructure along the depth to address this point. The idea that the long tail corresponds to diffusion in Harrison type B kinetic regime in analogy to grain boundary diffusion is unlikely, because the very slow bulk diffusion is not detectable in the present case (blue curve in Figure 3A).

Note that for the reference region of the sample (blue curve in Figure 3A), the deuterium fraction is enhanced by a factor of six over the natural background, in contrast to Figure 2B, where it is a factor of about two. This is likely caused by the fact that the pumping time of the SIMS analysis chamber might influence the determination of the exact D fraction due to the presence of residual hydrogen or water and resulting interferences with H. Further, measurements at different regions on the same sample were done by SIMS after pumping for a significant time in high vacuum. Some of the near-surface stored D may have diffused out prior to the analysis performed later. The near-surface sites are always filled if they have lower energy: D is then diffusing from the sample's in-depth region into these near-surface sites. The lateral surface inhomogeneity in D uptake (see Figure 4B) may also add to this fluctuation. Nevertheless, such fluctuations in the reference region are much less significant than the clear enhancement of D in the dislocation-rich region.

2.4 | Retention of deuterium in the dislocation-rich region

The 1 h incorporation of D at elevated temperature (400°C) as well as the low diffusivity obtained from Figure 3 suggests that once the D is incorporated in the dislocation-rich

region, the majority of D can be trapped and remain in the dislocation-rich region for a long time. To verify this, we performed additional time-of-flight SIMS (ToF-SIMS) measurements on the same sample after storing it under ambient conditions for about 300 days. The results in Figure 4 clearly illustrate D retention in the dislocation-rich region. Figure 4A shows the scratch tracks (dislocation-rich regions) on the left half and the reference regions on the right. The distribution of D fraction in Figure 4B correlates excellently with Figure 4A. Furthermore, a line profile (Figure 4C) is extracted from Figure 4B to display the D intensity profile as the distance goes from left to right, as in Figure 4B. Note the D intensity terminates almost abruptly at the end of the wear track, indicating that the dislocation distribution ends sharply at the end of the scratch track. This dislocation distribution was directly visualized by the Brinell indentation and dislocation etch pits analysis by Okafor et al.³²

It is noted that $X_D = I_D/(I_H + I_D)$ calculated from depth-integrated signal intensities after this long-time storage ($\sim 4.1 \times 10^{-3}$) is about one order of magnitude lower than the freshly exposed sample (Figure 2B), suggesting a continuous but very sluggish diffusion of D out of the sample. In the untreated area, X_D was found to be $\sim 4.5 \times 10^{-4}$, almost identical to the natural background, again confirming the impact of dislocations.

3 | DISCUSSIONS

3.1 | Increased hydrogen segregation at dislocations

Defects such as vacancies, dislocations, free surfaces, and grain boundaries can act as trapping sites for hydrogen, as widely established in crystalline solids with a majority of the evidence in metallic bulk materials and thin films.³³

Hydrogen ad- and absorption at these defects can lower the system's total strain energy.¹⁰ In the current case, the mechanically induced dislocations are effective for a much higher concentration of deuterium incorporation, as confirmed by the SIMS measurements. It is expected that the hydrogen uptake shall also be dependent on the dislocation densities, as will be investigated in detail in the future by tuning the dislocation densities in SrTiO₃.³⁴

3.2 | Thermal stability of the dislocations

As the D exposure was performed at 400°C for 1 h, it raises the concern whether the dislocations generated at room temperature have changed their configuration, namely, how thermally stable are these dislocations at 400°C for 1 h. Previous thermal treatment of the dislocations in SrTiO₃ suggests that these line defects persist and do not annihilate even up to 1200°C.^{35,36} Negm et al.³⁵ showed evidence of dislocation motion and density increase subjected to annealing at 1100°C for 1 h, followed by furnace cooling. To further examine the thermal stability of dislocations, following the method by Negm et al.,³⁵ we performed dislocation etch pit studies for samples treated at room temperature and up to 600°C (higher than 400°C in the current D exposure experiment) for 1 h. The etch pits analysis for dislocations confirms that no change of the dislocation structures in the surface region was observed at temperatures up to 600°C (see Figure S1). A comprehensive analysis of the temperature-dependent dislocation structure evolution merits an independent study and goes beyond the scope of this work.

3.3 | Impact of oxygen vacancies

Though the focus of this work is hydrogen-dislocation interaction, it is pertinent to consider the impact of oxygen vacancies as the oxide samples were exposed to a hydrogen-rich environment at elevated temperatures, and oxygen vacancies can be favorable trapping sites for hydrogen. Although commercially undoped SrTiO₃ is oxygen vacancy rich due to the tracer elements acting mostly as acceptor dopants,³⁷ these oxygen vacancies in the reference sample are not relevant for the current hydrogen/deuterium detection as evidenced by the benchmarking SIMS measurement in Figure 2.

However, with high-density dislocations mechanically generated in SrTiO₃, complexity is expected as previous reports suggest that the dislocations in SrTiO₃ are easy to reduce,³⁶ and the dislocation cores are oxygen deficient.^{38–41} Rodenbücher et al.^{42,43} investigated the mechanically induced dislocations and their electrical con-

ductivities, and their results suggest a strong interaction between dislocations and oxygen vacancies formed due to reduction, with the latter being locally compensated by electrons. The increased concentration of oxygen vacancies bonded to dislocations in SrTiO₃ may be responsible for the low diffusivity evaluated in Section 2, as these oxygen vacancies can act as effective trapping sites. The possible symbiosis of the dislocations and oxygen vacancies in SrTiO₃, together with the challenge in quantifying the oxygen vacancy concentrations in oxides,^{28,44} makes it difficult at this stage to experimentally decouple these two types of defects to allow for *pure* dislocation-hydrogen interaction, which we expect that positron annihilation lifetime spectroscopy⁴⁵ coupled with *ab initio* simulation may shed new light on it.

3.4 | Surface roughness

Note that the scratching approach using the Brinell indenter has altered the sample surface roughness. Compared to the reference sample with an average surface roughness of <1 nm, the change in the surface roughness after scratching is twofold: inside each individual scratch track and between the scratch tracks. Atomic force microscopy measurement of an area of 5 μm × 5 μm yields an average surface roughness of ~10 nm inside the scratch track, whereas the laser microscopy image presents a maximum scratch track depth of ~300 nm over a width of ~130 μm for each scratch track with 10 passes. Therefore, we consider it nominally flat inside the wear track, whereas the ridges between each two scratch tracks are clearly visible (see Figure 1B). However, the regions (where the ridges are) have not only the change in the surface roughness but also a lower dislocation density, and both factors together result in a lower D concentration, as evidenced in Figure 4A,B. Future work shall consider using an additional careful vibrational polishing step after the Brinell indenter scratching to reduce the surface roughness in order to exclude the surface roughness on D incorporation.

4 | CONCLUSION

Mechanically engineered large area (~2.5 × 2.5 mm²) with high-density dislocations (up to ~10¹⁴/m²) in nominally undoped single-crystal SrTiO₃ without forming cracks, sub-grain boundaries, or amorphous phases allows the probing of the hydrogen response to dislocations via SIMS measurements, using deuterium as tracer. The high-density dislocations generated at room temperature remain thermally stable at least up to 600°C for 1 h, and

they host a much higher relative deuterium concentration by a factor of ~ 100 compared to the reference sample. A diffusivity of deuterium with $\sim 2.7 \times 10^{17} \text{ m}^2/\text{s}$ has been obtained in the dislocation-rich region. Though this value is rather low, the findings can be relevant for hydrogen production and proton-exchanging oxide ceramics if the dislocation mesostructure can be further tuned to enhance the diffusivity. Open questions remain particularly concerning the impact of different dislocation densities, dislocation structures, hydrogen-induced defects,⁴⁶ and their interaction with other defects, for example, oxygen vacancies, dislocations, and interfaces on hydrogen uptake and diffusion.

ACKNOWLEDGMENTS

Xufei Fang, Maria Vrellou, and Christoph Kirchlechner acknowledge the financial support by the European Research Council (ERC Consolidator Grant, project TRITIME, Grant No. 101043969). Xufei Fang is also funded by the ERC (ERC Starting Grant, project MECERDIS, Grant No. 101076167) and the YIN Grant at Karlsruhe Institute of Technology. Views and opinions expressed are, however, those of the authors only and do not necessarily reflect those of the European Union or the European Research Council. Neither the European Union nor the granting authority can be held responsible for them. We thank A. Frisch for the optical image of the plastic zone and C. Kofahl for the annealing experiments in D_2O . This work was partly carried out with the support of the Karlsruhe Nano Micro Facility (KNMFi, www.knmf.kit.edu), a Helmholtz Research Infrastructure at Karlsruhe Institute of Technology (KIT, www.kit.edu). This work was also partly carried out with the support of the Joint Laboratory Model and Data-driven Materials Characterization (JL MDMC), a cross-center platform of the Helmholtz Association.

Open access funding enabled and organized by Projekt DEAL.

CONFLICT OF INTEREST STATEMENT

The authors declare no conflicts of interest.

DATA AVAILABILITY STATEMENT

The related data for this publication have been provided in the manuscript or in the Supporting Information section.

ORCID

Xufei Fang  <https://orcid.org/0000-0002-3887-0111>

REFERENCES

- El-Zoka AA, Stephenson LT, Kim SH, Gault B, Raabe D. The fate of water in hydrogen-based iron oxide reduction. *Adv Sci*. 2023;10(24):e2300626.
- Chung HW, Cladek B, Hsiao Y-Y, Hu Y-Y, Page K, Perry NH, et al. Hydrogen in energy and information sciences. *MRS Bull*. 2024;49:1–16.
- Ebert JN, Jennings D, Guillon O, Rheinheimer W. Black-light sintering of BaZrO_3 -based proton conductors. *Scr Mater*. 2025;256:116414.
- Kindelmann M, Escolastico S, Almar L, Vayyala A, Jennings D, Deibert W, et al. Highly conductive grain boundaries in cold-sintered barium zirconate-based proton conductors. *J Mater Chem A*. 2024;12(7):3977–88.
- Frisch A, Okafor C, Preuß O, Zhang J, Matsunaga K, Nakamura A, et al. Room-temperature dislocation plasticity in ceramics: methods, materials, and mechanisms. *J Am Ceram Soc*. 2025;108:e20575.
- Szot K, Rodenbücher C, Bihlmayer G, Speier W, Ishikawa R, Shibata N, et al. Influence of dislocations in transition metal oxides on selected physical and chemical properties. *Crystals*. 2018;8:241–317.
- Höfling M, Zhou X, Riemer LM, Bruder E, Liu B, Zhou L, et al. Control of polarization in bulk ferroelectrics by mechanical dislocation imprint. *Science*. 2021;372:961–64.
- Fang X. Mechanical tailoring of dislocations in ceramics at room temperature: a perspective. *J Am Ceram Soc*. 2024;107(3):1425–47.
- Fang X, Nakamura A, Rödel J. Deform to perform: dislocation-tuned properties of ceramics. *ACerS Bull*. 2023;102(5):24–29.
- Pundt A, Wagner S. Hydrogen interactions with defects in materials. *Chem. Ing. Tech*. 2024;96(1–2):182–91.
- Ren P, Song M, Lee J, Zheng J, Lu Z, Engelhard M, et al. Edge dislocations induce improved photocatalytic efficiency of colored TiO_2 . *Adv Mater Interfaces*. 2019;6:1901121.
- Zhang Y, Feng K, Song M, Xiang S, Zhao Y, Gong H, et al. Dislocation-engineered piezocatalytic water splitting in single-crystal BaTiO_3 . *Energy Environ Sci*. 2025;18:602–12.
- Liu Z, Zarotti F, Shi Y, Yang N. Dislocations promoted A-site nonstoichiometry and their impacts on the proton transport properties of epitaxial barium zirconate thin films. *J Phys Chem C*. 2019;123:20698–704.
- Felici R, Aruta C, Yang N, Zarotti F, Foglietti V, Cantoni C, et al. Regular network of misfit dislocations at the $\text{BaZr}_{0.8}\text{Y}_{0.2}\text{O}_{3-x}/\text{NdGaO}_3$ interface and its role in proton conductivity. *Phys Status Solidi*. 2018;256(3):1800217.
- Deibert W, Ivanova ME, Huang Y, Merkle R, Maier J, Meulenberg WA. Fabrication of multi-layered structures for proton conducting ceramic cells. *J Mater Chem A*. 2022;10(5):2362–73.
- Escolástico S, Ivanova M, Solís C, Roitsch S, Meulenberg WA, Serra JM. Improvement of transport properties and hydrogen permeation of chemically-stable proton-conducting oxides based on the system $\text{BaZr}_{1-x-y}\text{Y}_x\text{M}_y\text{O}_{3-\delta}$. *RSC Adv*. 2012;2(11):4932–43.
- Brunner D, Taeri-Baghdarani S, Sigle W, Rühle M. Surprising results of a study on the plasticity in strontium titanate. *J Am Ceram Soc*. 2001;84(5):1161–63.
- Fang X, Lu W, Zhang J, Minnert C, Hou J, Bruns S, et al. Harvesting room-temperature plasticity in ceramics by mechanically seeded dislocations. *Mater Today*. 2025;82:81–91.

19. Fang X, Preuß O, Breckner P, Zhang J, Lu W. Engineering dislocation-rich plastic zones in ceramics via room-temperature scratching. *J Am Ceram Soc.* 2023;106:4540–45.
20. Okafor C, Ding K, Preuß O, Khansur N, Rheinheimer W, Fang X. Near-surface plastic deformation in polycrystalline SrTiO₃ via room-temperature cyclic Brinell indentation. *J Am Ceram Soc.* 2024;107:6715–28.
21. Fang X, Ding K, Minnert C, Nakamura A, Durst K. Dislocation-based crack initiation and propagation in single-crystal SrTiO₃. *J Mater Sci.* 2021;56:5479–92.
22. Javaid F, Bruder E, Durst K. Indentation size effect and dislocation structure evolution in (001) oriented SrTiO₃ Berkovich indentations: HR-EBSD and etch-pit analysis. *Acta Mater.* 2017;139:1–10.
23. Dai JY, Pang GKH, Lee PF, Lam HK, Wu WB, Chan HLW, et al. Ambient-temperature incorporated hydrogen in Nb:SrTiO₃ single crystals. *Appl Phys Lett.* 2003;82(19):3296–98.
24. Waser R. Solubility of hydrogen defects in doped and undoped BaTiO₃. *J Am Ceram Soc.* 1988;71(1):58–63.
25. Sears VF. Neutron scattering lengths and cross sections. *Neutron News.* 2006;3(3):26–37.
26. Szot K, Speier W, Herion J, Freiburg C. Restructuring of the surface region in SrTiO₃. *Appl Phys A.* 1997;64:55–59.
27. Weber ML, Smid B, Breuer U, Rose MA, Menzler NH, Dittmann R, et al. Space charge governs the kinetics of metal exsolution. *Nat Mater.* 2024;23(3):406–13.
28. Stich S, Ding K, Muhammad QK, Porz L, Minnert C, Rheinheimer W, et al. Room-temperature dislocation plasticity in SrTiO₃ tuned by defect chemistry. *J Am Ceram Soc.* 2022;105:1318–29.
29. Dörrer L, Tüchel P, Hüger E, Heller R, Schmidt H. Hydrogen diffusion in proton-exchanged lithium niobate single crystals. *J Appl Phys.* 2021;129(13):135105.
30. Crank J. The mathematics of diffusion. 2nd ed. Oxford: Clarendon Press; 1975.
31. Dörrer L, Heller R, Schmidt H. Tracer diffusion in proton-exchanged congruent LiNbO₃ crystals as a function of hydrogen content. *Phys Chem Chem Phys.* 2022;24(26):16139–47.
32. Okafor C, Ding K, Zhou X, Durst K, Rödel J, Fang X. Mechanical tailoring of dislocation densities in SrTiO₃ at room temperature. *J Am Ceram Soc.* 2022;105:2399–402.
33. Pundt A, Kirchheim R. Hydrogen in metals: microstructural aspects. *Annu Rev Mater Res.* 2006;36(1):555–608.
34. Salem MN, Ding K, Rödel J, Fang X. Thermally enhanced dislocation density improves both hardness and fracture toughness in single-crystal SrTiO₃. *J Am Ceram Soc.* 2023;106:1344–55.
35. Zhang J, Fang X, Lu W. Impact of dislocation densities on the microscale strength of single-crystal strontium titanate. *Acta Mater.* 2025;291:121004.
36. Adepallo KK., Yang J, Maier J, Tuller HL, Yildiz B. Tunable oxygen diffusion and electronic conduction in SrTiO₃ by dislocation-induced space charge fields. *Adv Funct Mater.* 2017;27(22):1700243.
37. De Souza RA. Oxygen diffusion in SrTiO₃ and related perovskite oxides. *Adv Funct Mater.* 2015;25(40):6326–42.
38. Jia CL, Thust A, Urban K. Atomic-scale analysis of the oxygen configuration at a SrTiO₃ dislocation core. *Phys Rev Lett.* 2005;95:225506.
39. Jia CL, Houben L, Urban K. Atom vacancies at a screw dislocation core in SrTiO₃. *Philos Mag Lett.* 2006;86(11):683–90.
40. Choi S-Y, Kim SD, Choi M, Lee HS, Ryu J, Shibata N, et al., Assessment of strain-generated oxygen vacancies using SrTiO₃ bicrystals. *Nano Lett.* 2015, 2015(15):4129–34.
41. Gao P, Ishikawa R, Feng B, Kumamoto A, Shibata N, Ikuhara Y. Atomic-scale structure relaxation, chemistry and charge distribution of dislocation cores in SrTiO₃. *Ultramicroscopy.* 2018;184:217–24.
42. Rodenbücher C, Balin K, Wojtyniak M, Besmehn A, Korte C, Szot K. Preferential chemical oxygen diffusion along dislocation networks in SrTiO₃. *J Am Ceram Soc.* 2025;108:e20310.
43. Rodenbücher C, Bihlmayer G, Korte C, Szot K. Gliding of conducting dislocations in SrTiO₃ at room temperature: why oxygen vacancies are strongly bound to the cores of dislocations. *APL Mater.* 2023;11:021108.
44. Gunkel F, Christensen DV, Chen YZ, Pryds N. Oxygen vacancies: the (in)visible friend of oxide electronics. *Appl Phys Lett.* 2020;116(12):120505.
45. Elsayed M, Staab TEM, Čížek J, Krause-Rehberg R. Monovacancy-hydrogen interaction in pure aluminum: experimental and ab-initio theoretical positron annihilation study. *Acta Mater.* 2023;248:118770.
46. Sotoudeh M, Bongers-Loth MD, Roddatis V, Čížek J, Nowak C, Wenderoth M, et al. Hydrogen-related defects in titanium dioxide at the interface to palladium. *Phys Rev Mater.* 2021;5(12):125801.

SUPPORTING INFORMATION

Additional supporting information can be found online in the Supporting Information section at the end of this article.

How to cite this article: Fang X, Dörrer L, Korneychuk S, Vrellou M, Welle A, Wagner S, et al. Hydrogen response to high-density dislocations in bulk perovskite oxide SrTiO₃. *J Am Ceram Soc.* 2025;e70291. <https://doi.org/10.1111/jace.70291>